Braiding errors in interacting Majorana quantum wires

Michael Sekania,[1,2,3] Stephan Plugge,[4] Martin Greiter,[1] Ronny Thomale,[1] and Peter Schmitteckert[1,4]
[1]*Institute for Theoretical Physics and Astrophysics, Julius-Maximilian University of Würzburg, Am Hubland, 97074 Würzburg, Germany*
[2]*Center for Electronic Correlations and Magnetism, Institute of Physics, University of Augsburg, 86135 Augsburg, Germany*
[3]*Andronikashvili Institute of Physics, Tamarashvili 6, 0177 Tbilisi, Georgia*
[4]*Institut für Theoretische Physik, Heinrich-Heine-Universität, 40225 Düsseldorf, Germany*
(Received 17 March 2017; published 19 September 2017)

Avenues of Majorana bound states (MBSs) have become one of the primary directions towards a possible realization of topological quantum computation. For a Y junction of Kitaev quantum wires, we numerically investigate the braiding of MBSs while considering the full quasiparticle background. The two central sources of braiding errors are found to be the fidelity loss due to the incomplete adiabaticity of the braiding operation as well as the finite hybridization of the MBSs. The explicit extraction of the braiding phase from the full many-particle states allows us to analyze the breakdown of the independent-particle picture of Majorana braiding. Furthermore, we find nearest-neighbor interactions to significantly affect the braiding performance for better or worse, depending on the sign and magnitude of the coupling.

DOI: 10.1103/PhysRevB.96.094307

I. INTRODUCTION

Topological quantum states of matter have become one of the most vibrant fields of contemporary condensed matter physics. One subbranch thereof, the search for realizations of topological quantum computation, has decisively fueled the interest, both from theory and experiment, to address manifold scenarios of this kind. Among them, Majorana bound states (MBSs) have been attracting pivotal attention in recent years [1–4]. While Majorana-type quasiparticles have been previously addressed in the context of the fractional quantum Hall effect [5,6], unconventional superconductivity [6–8], and spin liquids [9,10], the proposal by Fu and Kane [11] to employ the conventional superconducting proximity effect to stabilize MBSs in vortex cores at the surface of a topological insulator unleashed a remarkable body of research that has brought the detection and manipulation of MBSs closer to reality. After crucial progress towards simpler realizations of proximity-induced topological superconducting phases [12–14], several experimental groups have reported increasingly compelling evidence for the observation of Majorana zero modes in semiconductor nanowires and iron atomic chains that are coupled to a bulk superconductor [15–25]. The unambiguous detection of a MBS, however, has so far remained elusive, and parity-changing quasiparticle poisoning through single-particle tunneling into the wire or chain likewise constitutes a major challenge. One crucial experimental finding in favor of the existence of Majorana zero modes would be a braiding experiment [26–29], revealing their nontrivial braiding statistics, and showing the path to more complex multi-MBS protocols.

A plethora of approaches is currently underway towards the realization of topological quantum computation in networks of semiconductor nanowires that are proximity coupled to a superconductor [29–36]. Alternative routes include the aforementioned proximitized topological-insulator surfaces [11,37,38], and atomic chains [14,28] or cold-atom setups [39,40], where the originally envisioned lattice realizations of topological superconductivity [7] are more directly accessible. Given the amount of different obstacles still to overcome, it is hard to predict which direction will lead to success. At the current stage of the field, it thus appears worthwhile to follow up on several of these directions at the same time: New results on any given approach will offer guidance for inevitable refinements of the others.

In this paper, we numerically analyze the braiding process of MBSs in a minimal model of an interacting wire network. To this end we define a Y junction of three Kitaev chains [7] in which we investigate the controlled time evolution of a single pair of MBSs as the most elementary braiding operation. We employ time-dependent on-site potentials to locally drive the system in and out of the topologically nontrivial phase, which hence allows us to spatially move the MBSs [26]. In particular, we consider unitary time evolution of initially prepared pure states, and analyze the absolute value (fidelity F) and the relative phase ϕ of the overlap between the initial and time-evolved states. The potential-manipulation protocol is analyzed to decrease nonadiabatic effects.

The use of exact diagonalization allows us to systematically identify the different sources of braiding errors. Since we keep the full Hilbert space during the braiding operation, the measured fidelities and phases are not influenced by implicit assumptions or restrictions. In addition, this allows us to extract explicitly the geometric exchange "braiding" phase acquired during the execution of the braid, directly encoding the non-Abelian statistics of MBSs. By varying the superconducting wire bulk gap, we then find how the localization length of the individual Majorana zero modes as well as the resulting MBSs' hybridization affect the braiding operation. Finally, interactions in the wires, modeled by a nearest-neighbor density-density coupling [41–43], are found to predominantly affect the braiding operation through its impact on the wire bulk gap. Depending on the noninteracting gap versus hopping strength, for weak attractive (repulsive) interactions, the braiding operation is more stable due to an increase (decrease) of the effective superconducting gap and reduction of the MBS localization length. For strong attractive or repulsive nearest-neighbor coupling, the interactions have a negative impact on the braiding performance, where ultimately the topological phase becomes inaccessible altogether [41–43].

II. KITAEV CHAIN

The (interacting) Kitaev model is the most elementary system exhibiting MBSs [7,41]. It is given by the Hamiltonian [44,45]

$$H = \sum_{i=1}^{L-1}(Jc_i^\dagger c_{i+1} + \Delta c_i^\dagger c_{i+1}^\dagger + \text{H.c.}) + \sum_{i=1}^{L}\mu_i n_i + \sum_{i=1}^{L-1} V n_i n_{i+1}, \quad (1)$$

where $c_i^\dagger$ (c_i) is a creation (annihilation) operator of the spinless fermion on site i and $n_i = c_i^\dagger c_i$ is the density operator. J denotes the nearest-neighbor hopping amplitude, $\Delta = |\Delta|e^{i\varphi}$ the p-wave superconducting pairing amplitude with phase φ, V the strength of the nearest-neighbor interaction, and μ_i the site-dependent potential. The superconducting pairing term breaks $U(1)$ fermion number symmetry down to $\mathbb{Z}_2$ (parity conservation), where the two parity sectors will be denoted even (e) and odd (o) below. Unless stated otherwise, we initially constrain ourselves to the noninteracting limit $V = 0$. The Kitaev chain features a topological trivial and nontrivial phase for $|\mu| > 2J$ and $|\mu| \leq 2J$, respectively, so long as $|\Delta| > 0$ [1,7]. For the ideal parameter set $\mu = 0$, $|\Delta| = J$, and hard wall boundary conditions, hence residing in the nontrivial regime, Hamiltonian (1) takes a particularly simple form in terms of a Majorana fermion representation $H = -J\sum_{j=1}^{L-1} i\gamma_{2j}\gamma_{2j+1}$, where $\gamma_{2j-1} = e^{i\varphi/2}c_j + e^{-i\varphi/2}c_j^\dagger$ and $\gamma_{2j} = (e^{i\varphi/2}c_j - e^{-i\varphi/2}c_j^\dagger)/i$ are real Majorana operators $\gamma_i^\dagger = \gamma_i$ obeying a Clifford algebra, $\{\gamma_i,\gamma_j\} = 2\delta_{ij}$. We observe that the first and last Majorana modes, residing on the first and last site, respectively, are decoupled from the rest of the fermionic chain. The corresponding Majorana operators $\gamma_1 \equiv \gamma_\text{L}$ and $\gamma_{2L} \equiv \gamma_\text{R}$ do not appear in the Hamiltonian, $[H,\gamma_\text{L}] = [H,\gamma_\text{R}] = 0$, and form a fermionic zero-energy mode comprising two individual Majorana (zero) modes localized on single sites at each end of the chain. After introducing a nonlocal fermionic operator $f = \frac{1}{2}(\gamma_\text{L} + i\gamma_\text{R})$, these zero-energy states can be identified with MBS eigenstates $f|0\rangle = 0$ and $f^\dagger|0\rangle = |1\rangle$, which reside in the middle of the effective bulk gap $4|\Delta|/J$. The states $|0\rangle$ and $|1\rangle$ also coincide with the parity eigenstates of the full fermionic chain, and can be associated with the ground-state wave functions of the Kitaev Hamiltonian Eq. (1) in the even (e) and odd (o) parity sector, respectively [46].

Away from this particular parameter set but still within the nontrivial regime, i.e., for $\mu = 0$ and $|\Delta| < J$, or $0 < \mu < 2J$ and $|\Delta| = J$, the Majorana zero modes develop an exponential tail extending into the bulk, yielding a small energy split of the two eigenstates previously located at zero energy (in different parity sectors). This splitting energy, usually referred to as MBS hybridization energy, decays exponentially with the distance between MBSs on a length scale governed by Δ (cf. Fig. 3). The protection offered by the bulk energy gap and spatial isolation of MBSs are the main stimuli for $|0\rangle$ and $|1\rangle$ to serve as a basis for the sought-after topological qubit. As we show below, targeting the entire Hilbert space—and not only a subspace of subgap Majorana states in terms of an effective low-energy theory as conventionally assumed [26–35,37–40,47–53]—is essential when braiding manipulations are performed on finite time scales, i.e., nonadiabatically, and in finite-size systems. Preceding works undertook steps in this direction [54–56], but attempted to search the errors in an effective low-energy (Majorana) picture.

Here, via a sequence of predefined exact manipulations of potentials μ_i of Hamiltonian (1), we perform a braiding operation imposed on an initially prepared set of MBSs [26]. Such manipulations employ unitary but in general nonadiabatic dynamics. This implementation requires a way to (i) dislocate MBSs without destroying them or creating new ones, (ii) realize a system geometry that allows one to exchange Majorana modes while keeping their overlap exponentially small during the entire braiding process, and (iii) provide an exchange process that gives fidelity, taken as the overlap between initial and final states, close to unity.

At the elementary level of our description, the goal is not to define the optimal exchange protocol applied to a realistic setup for topological quantum computation (though we made sure to select a favorable implementation among several "simple" test routines). Rather, for the simplest braiding operation possible, we intend to identify the time scale and conditions under which it is feasible to perform a braiding with the desired fidelity and braid-phase accuracy. For an analysis of tailor-made braiding protocols and possible drawbacks or limitations thereof, based on effective models of the low-energy (Majorana) sector of the system, see Refs. [52,53,56].

III. Y JUNCTION

The minimal geometry required for the exchange "braiding" of MBSs is a junction with three legs (trijunction) [1,26]. It can be formed by connecting three Kitaev chains Eq. (1) (later referred to as junction legs) to an additional connecting junction site at $i = 0$, which otherwise witnesses parameter sets identical to the respective adjacent leg,

$$\begin{aligned} H_\text{Y} = {} & \mu_0 c_0^\dagger c_0 \\ & + \sum_{n=1}^{3}\Bigg[\left(J^{(n)}c_0^\dagger c_1^{(n)} + \Delta^{(n)}c_0^\dagger c_1^{\dagger,(n)} + \text{H.c.}\right) + V^{(n)}n_0 n_1^{(n)} \\ & + \sum_{i=1}^{L^{(n)}-1}\left(J^{(n)}c_i^{\dagger,(n)}c_{i+1}^{(n)} + \Delta^{(n)}c_i^{\dagger,(n)}c_{i+1}^{\dagger,(n)} + \text{H.c.}\right) \\ & + \sum_{i=1}^{L^{(n)}-1} V^{(n)}n_i^{(n)}n_{i+1}^{(n)} + \sum_{i=1}^{L^{(n)}}\mu_i^{(n)}n_i^{(n)}\Bigg]. \end{aligned} \quad (2)$$

In general, one may choose different p-wave pairing terms $\Delta^{(n)}$ and hopping amplitudes $J^{(n)}$ in each leg of the Y junction. For simplicity, we here assume that $J^{(n)} = 1$ (thus setting the reference scale in plots and equations below), $\Delta^{(1)} = -\Delta$, $\Delta^{(2)} = \Delta\, e^{i\varphi_2}$, and $\Delta^{(3)} = \Delta\, e^{i\varphi_3}$, with a real pairing amplitude $\Delta > 0$. The superconducting pairing phase φ_n is chosen to coincide with the corresponding geometric angle of the nth leg of the Y junction (cf. Fig. 1). This type of triplet pairing could, for example, be realized in a Y junction placed in proximity to a chiral p-wave superconductor [49]. The connection of two

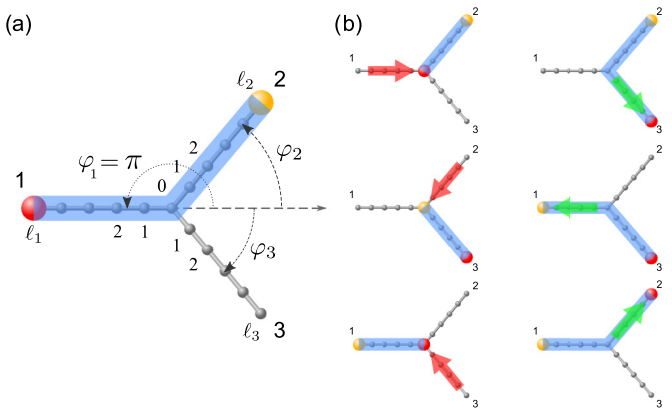

FIG. 1. Y junction of three Kitaev chains and the braiding protocol considered here. MBSs, depicted by red and yellow spheres, reside at the ends of segments with a topological nontrivial phase (highlighted by blue tubes). (a) The initial state. Geometric angles φ_i also correspond to the superconducting pairing phases of the respective junction legs. (b) The exchange "braiding" protocol (left to right and top to bottom), as in Ref. [26]. Red (green) arrows indicate displacements of MBSs by contraction (extension) of the topological chain segment, implemented by locally ramping up (down) the local potential over the critical value $\mu_c = 2J$. At the end of the braiding protocol (right picture, bottom row), the same chain segments as in the initial state reside in the topological phase, but the MBSs have been exchanged.

Kitaev chain legs, both of which are in the topological (trivial) phase, produces a single segment residing in the topological (trivial) phase; unless the mutual phase difference between the pairing terms of these chains equals exactly $\varphi_i - \varphi_j = 0$, MBSs on the connecting site fuse, and the entire segment ends up with the two leftover MBS residing on the free ends of the new, larger topological segment [26]. If the mutual phase, however, is exactly zero, MBSs on the connecting site do not fuse and the joint segment maintains all four Majorana zero modes (one from each end of the initial chains)—a case we intentionally avoid in the following. In addition, we restrict our studies to clean systems, avoiding additional complications arising from disorder [57].

By ramping up the on-site potentials over the critical value of $\mu_c = 2J$ starting from one end of the topological segment (i.e., at the location of a Majorana zero mode), locally one drives the system into the trivial phase. As the ramp of potentials is successively carried out along the chain, one thus continuously displaces the MBS alongside with the trivial-topological domain wall. This action can be undone by again lowering the local potentials below the critical value, and switching the chosen sites back from the trivial to topological phase. Finally, concerting such ramping procedures in sequences across all three junction legs, one can create the desired Majorana zero mode exchange or braiding operation [26]. This process is schematically depicted in Fig. 1. We will only study Y junctions with legs of equal length $L^{(n)} = \ell$, and take $\varphi_2 = -\varphi_3 = \varphi$. The initially homogeneous potentials in the junction legs are $\mu^{(1)} = \mu^{(2)} = 0$ and $\mu^{(3)} = 2\mu_c$, meaning that legs 1 and 2 reside in the topological, and leg 3 in the trivial phase. In passing, we note that since the time evolution of an initial state prepared in this way fixes a time direction, there is a subtle time-reversal symmetry breaking appearing in the braiding setup, as seen by reversing the sign of φ in the time evolution. We thus only consider $\varphi > 0$ in the following.

IV. RAMPING PROTOCOL

We investigated several ramping protocols for the successive time variation of the on-site potentials $\mu_i^{(n)}(t)$. The results were found by employing a sine-squared ramp defined as

$$\mu_j^{(n)}(\tau) = 2\mu_c\, m\left(\frac{\tau}{T}[1+\alpha(\ell-1)] - \alpha(\ell-j)\right), \quad (3)$$

where $\tau \in [0,T]$ denotes the time during the respective ramp-up protocol step in Fig. 1, α is a delay coefficient, and we used the scalar function

$$m(q) = \sin^2\left(\frac{\pi}{2}r(q)\right). \quad (4)$$

Here, $r(q)$ is a linear ramp of unit height and duration

$$r(q) = \min\left[\max(q,0),1\right] = \begin{cases} 0, & q < 0, \\ q, & 0 \le q \le 1, \\ 1 & q > 1. \end{cases}$$

We also show results obtained by the simpler, linear "guillotine" ramp, $m(q) = r(q)$, where the smoothening by the sine-squared function in Eq. (4) is switched off. Both procedures raise the on-site potentials in the nth leg, containing ℓ sites, from $\mu_{\rm init}^{(n)} = 0$ to $\mu_{\rm f}^{(n)} = 2\mu_c = 4J$ within the time period T. The time required to lift the on-site potential on each individual site is $T/[1+\alpha(\ell-1)]$, and the ramping is delayed by $\alpha T/[1+\alpha(\ell-1)]$ between consecutive sites. For a guillotine ramp, the modulations of local potentials are reminiscent of a guillotine knife passing a rectangular window (hence the name), and α is the inclination of the knife.

The delay coefficient (inclination) can be varied between $\alpha = 0$ and $\alpha = 1$, corresponding to a simultaneous ramp of all sites or a consecutive site-by-site ramping, respectively. In the following, we set $\alpha = 0.025$ and vary the time step T, where $\alpha^{-1}, T \gg \ell$ at all times, i.e., a small ramp delay (inclination) and slow ramp protocol. Finally, the ramp-down is implemented as an exact time reverse of the ramp-up protocol, with $\tau \to T - \tau$ in Eq. (3). The ramping (and hence braiding) protocol is accomplished numerically by replacing the continuous time evolution with a piecewise time-independent Hamiltonian

$$\mathcal{T} e^{-i\int_0^T H_{\rm Y}(t)dt} \to \mathcal{T}\prod_{j=0}^{N-1} e^{-i\Delta t\, H_{\rm Y}(j\Delta t)} \quad (5)$$

leading to the time-evolved state

$$\begin{aligned} |\psi(t+T)\rangle &= \mathcal{T} e^{-i\int_t^{t+T} H_{\rm Y}(\tau)d\tau}|\psi(t)\rangle \\ &= \left(\mathcal{T}\prod_{j=0}^{N-1} e^{-i H_{\rm Y}(t+j\Delta t)\Delta t}\right)|\psi(t)\rangle, \end{aligned} \quad (6)$$

where $\mathcal{T}$ is the time ordering operator, and $H_{\rm Y}(t)$ corresponds to Eq. (2) with the time-dependent local potential $\mu_j^{(n)} \to$

$\mu_j^{(n)}(t)$ given in Eq. (3). The time-step discretization $\Delta t/T \ll 1$ governs the accuracy of approximation of the continuous time-dependent Hamiltonian by a piecewise constant one, and is chosen sufficiently small against all energy scales of the problem, yielding a total of $N = T/\Delta t$ steps per braiding sweep in Fig. 1. We have checked that runs for each given parameter set are converged with respect to vanishing Δt. As such, the outlined braiding protocol demands a total (final) braiding time $t_f = 6T$, and performs a complete cyclic evolution in the parameter space of the Hamiltonian.

As braiding errors are detected, there are several parameters that can be used to control and alter the braiding process. The ramping speed can be controlled by the time period T required for each step of the protocol, and by the ramp delay/inclination α. Since the latter also determines the steepness of the trivial-topological domain wall propagating through the chain, generally, for steeper inclinations, a slower braiding velocity $\sim \ell/T$ with a larger time period T is required [50,51].

V. FIDELITY AND GEOMETRIC BRAIDING PHASE

In order to achieve an ideal braiding process, it is necessary (but not sufficient) that the fidelity between the initial and obtained final state equals unity. Since numerical simulations of the full Hilbert space are costly in general, and sampling the fidelity for many input states—in particular, if one is interested in longer braiding sequences—is not feasible, we propose to analyze the topological character and protection of braiding operations for the ground states of the two parity sectors. For this purpose, the braiding statistics are directly encoded in the relative geometric phase factor (the braiding phase) between final and initial states in the even- and odd-parity sector. Braiding errors then manifest both in deviations of the braiding fidelity from unity and of the braiding phase from $\pi/2$. Both quantities are accessible by considering input states $|0\rangle$ and $|1\rangle$ of the topological qubit, chosen as the ground states of $H_Y(t_0 = 0)$ Eq. (2) in the respective total-parity sector. [Note that transitions between even (e) and odd (o) total-parity states are forbidden under unitary time evolution Eq. (6) with a parity-conserving Hamiltonian Eq. (2).]

In order to quantify the fidelity loss during the braiding, we introduce the loss function

$$w_{\rm loss}(t_f) = 1 - F(t_f)^2 = 1 - |\langle\psi(t_f)|\psi(t_0)\rangle|^2, \qquad (7)$$

where $F(t_f) = |\langle\psi(t_f)|\psi(t_0)\rangle|$ is the fidelity for pure states [58], taken between the initial and final, time-evolved state. Note that zero loss (unit fidelity) does not necessarily imply that the overall process is adiabatic, however, a cyclic and completely adiabatic process should always yield $w_{\rm loss} = 0$. Similar measures, but with an adiabatically evolved state as a reference, have been used in Refs. [52,54]. The studies presented in Ref. [54], however, considered only the single-particle eigenstates of the MBS sector and investigated transitions among them. In the simple two-Majorana braiding setup of Fig. 1, after all, the states of different total parity are fully decoupled and do not mix.

In order to determine the braiding phase, note that the braiding protocol describes a cyclic evolution in the space of Hamiltonian parameters, where the Hamiltonian takes its original form at the end of the process, i.e., at time $t_f = 6T$. Assuming that the entire process is adiabatic, which implies that the time-evolving state always corresponds to an eigenstate of the instantaneous Hamiltonian, one can evaluate a Berry phase [59] acquired during this cyclic evolution of the system. Due to the finite ramping times, however, the braiding process in general is nonadiabatic and we find $w_{\rm loss}(t_f) > 0$. As a consequence, the Berry phase is not rigorously applicable. In addition, the finite fidelity error of the final state of the braiding shows that the obtained final state is not an eigenstate of the initial/final Hamiltonian, as the ground states in the fixed parity sectors are nondegenerate. The latter will also manifest in a nonconstant dynamical evolution of the acquired phase even after the system is evolved back to the initial Hamiltonian (cf. Fig. 2). Because quantum states that differ merely by a phase factor give rise to the same physics and the unitary time evolution of states under a continuous time-dependent Hamiltonian describes a smooth curve in the Hilbert space, one may employ the gauge- and parametrization-invariant functional [60,61]

$$\phi_g[C_0] = \arg\langle\psi(t_0)|\psi(t_f)\rangle - \mathrm{Im}\int_{t_0}^{t_f}\langle\psi(t)|\dot{\psi}(t)\rangle dt, \qquad (8)$$

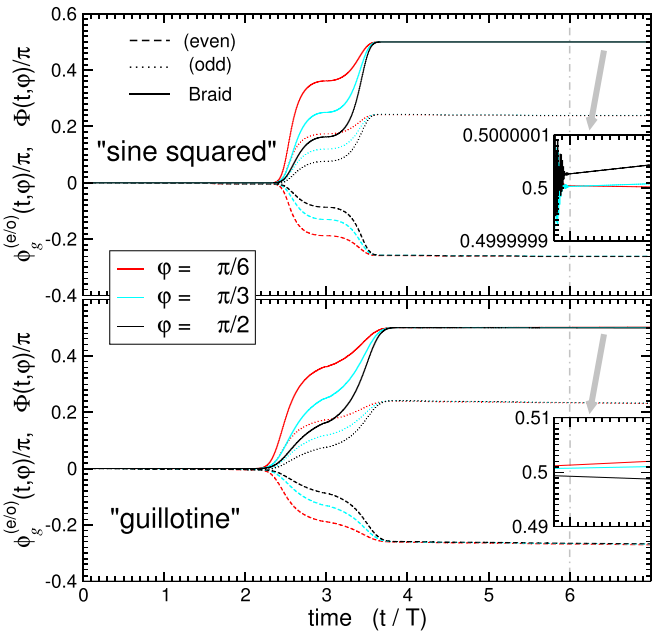

FIG. 2. Time evolution of the acquired exchange phases $\phi_g^{e/o}(t,\varphi)$ (dashed/dotted lines), and the phase difference $\Phi(t,\varphi)$ (solid lines) during the braiding protocol for sine-squared (top) and guillotine ramps (bottom). We consider a Y junction with equal-size legs $\ell = 5$, for triplet-pairing phases $\varphi = \pi/6, \pi/3, \pi/2$ and amplitude $\Delta = 1$. The braiding protocol takes a total time $t_f = 6T$, where we choose a time period $T = 750$ for each ramp-up/down step, with $\alpha = 0.025$. After complete execution of the braiding exchange, upon reaching $t = t_f$ (dashed-dotted vertical line), an extra time evolution of duration T is carried out with fixed Hamiltonian $H(t_f)$. The insets show the residual dynamic evolution of the exchange phase $\Phi(t)$, for $t \in [5.8T, 7T]$, zoomed in on the y scale.

which measures the geometrical phase for the smooth open curve of normalized (unit) vectors in the Hilbert space, $\mathcal{C}_0 = \{|\psi(t)\rangle \in \mathcal{N}_0 \mid t \in [t_0,t_\mathrm{f}] \subset \mathbb{R}\} \subset \mathcal{N}_0$. Here, $\mathcal{N}_0$ denotes the space of normalized vectors and C_0 is the projection of $\mathcal{C}_0$ to the so-called ray space (or projective Hilbert space), where members that differ only by a phase factor are regarded as equivalent [62]. Finally, since in our studies the ramping (and hence braiding) protocol is accomplished by the piecewise constant time-independent Hamiltonian Eqs. (5) and (6), C_0 is a continuous but generally not a smooth curve. To determine the geometric phase numerically we hence employ a discretized variant of the above functional [61],

$$\begin{aligned}\phi_\mathrm{g}[\tilde{C}_0] &= \arg(\langle\psi(t_0)|\psi(t_\mathrm{f})\rangle) - \arg\left(\prod_{j=0}^{N-1}\langle\psi(t_j)|\psi(t_{j+1})\rangle\right)\\ &= -\arg(\langle\psi(t_0)|\psi(t_1)\rangle\langle\psi(t_1)|\psi(t_2)\rangle\cdots\\ &\quad\cdots\langle\psi(t_{N-1})|\psi(t_\mathrm{f})\rangle\langle\psi(t_\mathrm{f})|\psi(t_0)\rangle),\end{aligned} \tag{9}$$

which measures the geometric phase for the closed $N+1$-sided polygon of unit vectors in the Hilbert space, $\tilde{\mathcal{C}}_0 = \{|\psi(t_j)\rangle \in \mathcal{N}_0 \mid t_j = t_0 + j\Delta t, j = 0,\ldots,N\}$, with $N = t_\mathrm{f}/\Delta t$. The closed polygon $\tilde{C}_0$ parametrizes the braiding protocol and corresponds to a projection of the time-ordered set $\tilde{\mathcal{C}}_0$ onto ray space. This expression, which is cyclically symmetric, is also referred to as the Bargmann vertex formula for the geometric phase. For the continuous limit, $\Delta t \to 0$ in Eqs. (5) and (6), the expression in Eq. (9) reduces to the continuous-time version in Eq. (8). We note that if the fidelity between the initial and final states is exactly one (zero loss), C_0 becomes a closed curve in ray space, and $\phi_\mathrm{g}[C_0]$ in Eq. (8) corresponds to the Aharonov-Anandan geometrical phase [63]. If the entire process is adiabatic, one recovers the conventional Berry phase [59] (for a discussion, cf. Ref. [61]). In terms of a physical interpretation, the first and second terms in Eqs. (8) and (9) correspond to the complete and the local, dynamic parts of the acquired phase, respectively. We thus explicitly exclude purely dynamic contributions, for example, those generated by the finite hybridization energy of MBSs [26,47,48], from our considerations. While in an actual application of braiding in Majorana-based quantum computation schemes [26–29], the (purely) dynamic and the geometric parts of the obtained total phase should be treated on equal footing (since both contribute to the resulting computational phase of the topological qubit), only the geometric part becomes truly universal. The latter then directly reflects the anyonic statistics encoded in the full many-body Hilbert space of the complex, in general interacting system given by Eqs. (1) and (2). As we will see below, this yields valuable information about the validity and possible shortcomings of simple Majorana toy models of topological superconducting systems [7,26–36].

VI. EXACT DIAGONALIZATION

The initial states $|e\rangle$ and $|o\rangle$ are chosen as the ground states of $H_\mathrm{Y}(t_0)$ in even and odd total-parity sectors, obtained through Davidson exact diagonalization [64]. The braiding is then carried out iteratively by applying the Arnoldi scheme [65] to the matrix exponential in Eq. (6). Since the time-dependent Hamiltonian conserves fermion parity, the simulation for each total-parity sector can be carried out separately. Further, while strictly speaking the geometric phase is only defined after the braiding process is carried out completely and a closed loop in parameter space is accomplished, it is convenient to define the exchange phase at arbitrary time t of the braiding process,

$$\Phi(t) = \phi_\mathrm{g}^o(t) - \phi_\mathrm{g}^e(t). \tag{10}$$

Here, $\phi_\mathrm{g}^e(t)$ and $\phi_\mathrm{g}^o(t)$ are the individual geometrical phases acquired during the time evolution of states $|e\rangle$ and $|o\rangle$. We note $|e\rangle \to e^{i\phi_\mathrm{g}^e(t)}|e\rangle$ and $|o\rangle \to e^{i\phi_\mathrm{g}^o(t)}|o\rangle$.

We now are equipped to study the symmetric Y junction with equal-size legs $\ell = 5$. Qualitatively similar results were found for leg sizes $\ell \leq 4$. At the ideal Kitaev point $\Delta = J = 1$, the lowest-energy (initial) states in the even- and odd-parity sector correspond to $|0\rangle$ and $|1\rangle$ states of the topological qubit, i.e., they differ in terms of the Majorana sector only. After the exchange "braiding" of Majorana modes, in general, both states will acquire different geometrical phases ϕ_g^e and ϕ_g^o. In an ideal case the accumulated many-body geometrical phase for $|0\rangle$ and $|1\rangle$ (and hence for $|e\rangle$ and $|o\rangle$) will only differ by a nontrivial phase stemming from the protected braiding exchange of Majoranas γ_L and γ_R. In Fig. 2 we show the time evolution of phases $\phi_\mathrm{g}^e(t,\varphi)$ and $\phi_\mathrm{g}^o(t,\varphi)$, as well as the phase difference $\Phi(t,\varphi)$ in Eq. (10), for sine-squared and guillotine ramp protocols and several superconducting pairing phases. Here, after finishing the braiding protocol at time $t_\mathrm{f} = 6T$, we continue the time evolution for yet another period T. In the fully adiabatic case, the geometrical phases in each parity sector—and hence the difference between them—should remain unchanged for times $t > t_\mathrm{f}$, i.e., when the braiding exchange has been executed completely. In our case, however, the phases keep evolving linearly in time (insets in Fig. 2). We wish to emphasize that this phase evolution is *not* due to purely dynamical phases as, e.g., caused by finite Majorana hybridization [47,48], which are explicitly excluded in Eq. (9). Instead, we can rationalize the continued nontrivial evolution by observing that the fidelity of the obtained states at time $t = t_\mathrm{f}$ is not exactly one, or, equivalently, the loss as defined in Eq. (7) is nonzero (cf. Fig. 4 and discussion). Since in the adiabatic (hence zero-loss) limit the system should have reached a state equivalent to the initial state but with the Majorana zero modes exchanged, this implies that, instead, the system no longer resides in an eigenstate of its Hamiltonian for $t \geq t_\mathrm{f}$. Such nonadiabatic spectral losses hence correspond to a leakage of wave-function weight out of the Majorana, and into the excited-state sector. Consequently, the state at $t \geq t_\mathrm{f}$—when projected to the (initial) qubit Hilbert space $\{|0\rangle,|1\rangle\}$—will "dephase" with time. This finding emphasizes the danger of nonadiabatic errors and excitations even in the most basic braiding experiments, and cannot be alleviated by just increasing the system size [55,56]. While the choice of φ changes the time dependence of the measured phase ϕ_g, as shown in Fig. 2, the value at t_f depends only weakly on φ in the range of $\varphi \in [\pi/6,\pi/2]$, and the residual evolution becomes negligible in the fully adiabatic limit. Therefore we will constrain ourselves to the symmetric case $\varphi = \pi/3$ in the following. Note that for the finite system size considered,

this corresponds to the largest minimum of the time-evolving protective gap among all other geometric configurations of Y junctions.

VII. BRAIDING ERRORS

There are several sources of errors that destroy the perfect quantization of the braiding phase during the nonadiabatic, unitary time evolution of the system. One is seen as a reduced fidelity due to the spectral losses (cf. Fig. 4 and the discussion above), which are expected to be larger for a smaller protective gap ($\sim\Delta$), lower ramp time T, and rougher ramp functions. Further, the condition of exponential localization of the two Majorana zero modes is invalidated when the MBS localization length becomes comparable with the chain size (see Fig. 3). In this case, the hybridization between MBSs is not exponentially small and the braiding phase encodes effects stemming from this hybridization. The minimal protective gap as well as Majorana localization length both depend on the p-wave pairing amplitude Δ. The localization length in the infinitely long Kitaev chain, for which exact results are easily obtained, is given by $\xi_\infty(\Delta) = 1/\ln\sqrt{(J+|\Delta|)/(J-|\Delta|)}$ in the case of $\mu = 0$. In Fig. 3(a) we show $\xi_\infty(\Delta)$ and the finite-length $\xi(\Delta, L)$ as a function of Δ. The latter is determined by fitting the weights of the fermionic representation of the MBSs to an exponentially decaying function modulated by Friedel oscillations with period π [42]. $L = 11$ and $L = 6$ chain sizes correspond to the maximal and minimal length of the topological regions during the braiding in the symmetric Y junction with equal-size legs $\ell = 5$ (cf. Fig. 1). Perfectly localized MBSs, $\xi \to 0$, are obtained at $J = \Delta = 1$. For $\Delta < 1$, MBSs acquire a finite width that increases with decreasing values of Δ, and the localization length $\xi(\Delta)$ diverges for vanishing Δ. We note that the numerical result $\xi(\Delta, L = 6)$ starts to deviate from $\xi_\infty(\Delta)$ at $\Delta \lesssim 0.5$, indicating that MBSs are no longer isolated and the independent-particle picture [8,26] for the edge modes breaks down. In Fig. 3(b) we show the MBS hybridization energy $\varepsilon(\Delta, L)$ for six, eight, and ten sites versus the pairing amplitude Δ. Combining the data corresponding to Figs. 3(a) and 3(b) in Fig. 3(c), we show that the scaled MBS hybridization energy $\varepsilon(\Delta, L)/4\Delta$ displays an exponential dependence on the scaled inverse localization length $L/\xi(\Delta, L)$ for $\xi(\Delta, L) \ll L$, with noticeable deviations for L being comparable to $\xi(\Delta, L)$.

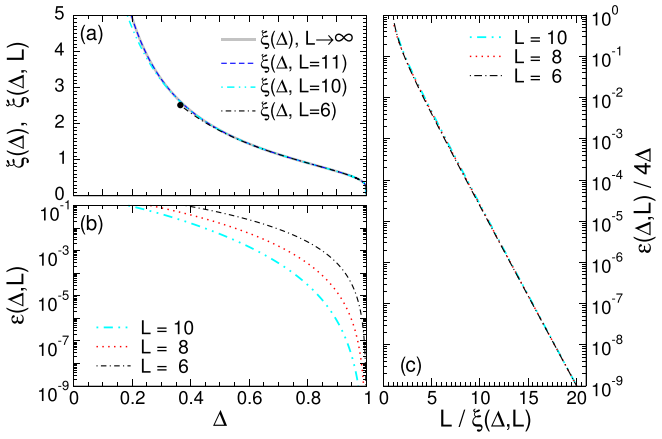

FIG. 3. Localization length ξ and hybridization energy ε of Majorana edge modes in a Kitaev chain with $\mu = 0$. (a) MBS localization length for infinite-size, $\xi(\Delta)$, and finite-size Kitaev chains, $\xi(\Delta, L)$, as a function of pairing amplitude Δ. Results for the infinitely long (bold gray curve) and finite Kitaev chains match closely already for modest $L = 11$ (dashed curve) and $L = 6$ (dashed-dotted curve). (b) MBS hybridization energy $\varepsilon(\Delta, L)$ for finite-size Kitaev chains. (c) Semilog plot of scaled MBS hybridization energy $\varepsilon(\Delta, L)/4\Delta$ vs scaled inverse localization length $L/\xi(\Delta, L)$. For comparable L and $\xi(\Delta, L)$ there is a clear deviation from the exponential dependence (upper left corner).

In Fig. 4 we show the braiding phase and fidelity losses as a function of the Majorana localization length $\xi(\Delta)$ for the two ramp protocols and various step times T. Data in Fig. 4 (bottom row) show that fidelity losses, Eq. (7), reduce by orders of magnitude upon increasing the ramping time period T from 250 to 3000. In addition, losses can be reduced significantly (by a power of 2) upon employing the smoother sine-squared ramp function (first derivative is continuous) instead of the simpler guillotine one (first derivative jumps), agreeing with the power-law scaling identified by Knapp *et al.* [56]. Similarly, nonadiabatic effects measured directly in the exchange phase Eq. (10) (see Fig. 4, top), which can be assessed by the strength of phase variations as a function of the braiding parameters (i.e., the sensitivity of the braiding phase against small deviations in the protocol), become smaller. In the adiabatic limit for large T, these fluctuations become negligible and one obtains smooth curves $\Phi(\xi, \Delta, \ldots)$. In addition to the guillotine and sine-squared ramping, we have also used the infinitely differentiable function $m(r) = e^{-1/r}/(e^{-1/r} + e^{-1/(1-r)})$ leading to the same phase as the sine-squared protocol, while the fidelity errors are even smaller.

The braiding phase is stable and closest to $\pi/2$, independent of T, for the ideal parameter set $\Delta = J = 1$. As expected, for nonideal values $\Delta < 1$, stable braiding phases are obtained only for larger times T. There are, however, significant deviations from the desired $\pi/2$ braiding phase starting from $\xi > 1$ (corresponding to $\Delta < 0.7$), which persist largely independent of the protocol time T or smoothness of the ramp function. These can be identified with a breakdown of the independent-particle picture of Majorana braiding, where ideal braiding statistics no longer apply. We emphasize again that these phase deviations are *not* a remnant of purely dynamic errors, as we only consider the geometric part of the exchange phase in Eq. (9). Further, even though the braiding process appears quasiadiabatic for $T \geq 500$ (or $T \geq 1500$ for the guillotine ramp), only the exchange phase itself encodes this dramatic breakdown of braiding, while fidelity losses even for large ξ are substantially smaller compared to faster braiding. Matching the Majorana wave-function weights or checking for adiabacity alone may thus be too loose a criterion for successful Majorana braiding protocols [52,54].

VIII. PROJECTED EVOLUTION

In order to clarify the results in the slow (large T) braiding limit, we also performed simulations where we project, after each time step, the time-evolved state on the ground state of

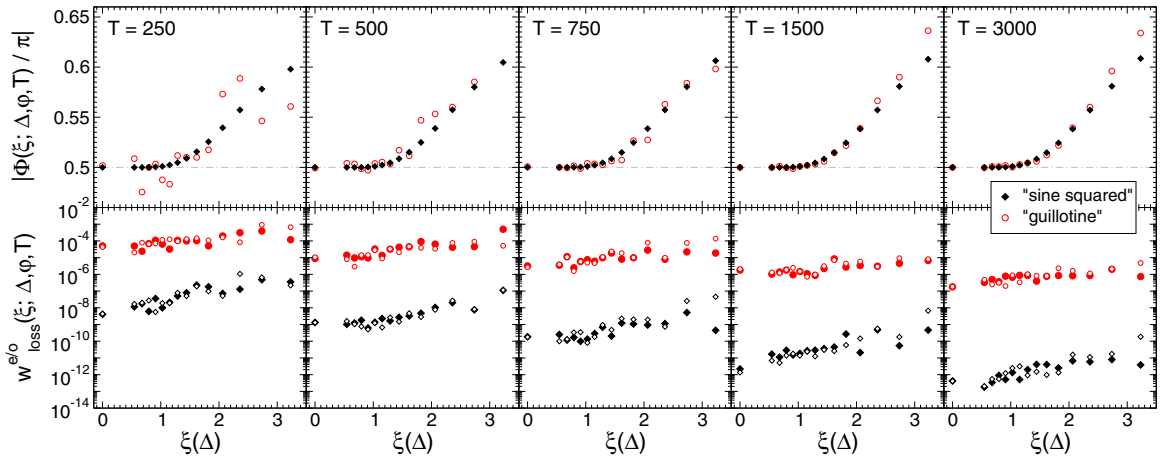

FIG. 4. Exchange phase $\Phi(\xi;\Delta,\varphi,T)$ (top row) and loss of fidelity $w^{e/o}_{\rm loss}(\xi;\Delta,\varphi,T)$ (bottom row) vs MBS localization length $\xi(\Delta)$, for sine-squared (black diamonds) and guillotine ramps (red circles). We consider a symmetric Y junction ($\varphi=\pi/3$) with equal-size legs $\ell=5$. Plots from left to right correspond to execution of the braiding protocol with ramping time periods of $T=250$, 500, 750, 1500, and 3000, respectively, with $\alpha=0.025$. Data points (left to right) for each plot correspond to pairing amplitudes $\Delta=1.0,\ldots,0.3$ in steps 0.05, which translates to increasing MBS localization length $\xi(\Delta)$ from left to right. The loss of fidelity (bottom row) in even and odd total-parity sectors is shown by solid and open symbols, respectively.

the instantaneous time-independent Hamiltonian. In addition, we performed a state tracking as described in Ref. [66], which resembles the previous approach provided no ground-state level crossings occur. Finally, we also evaluated the geometrical phase, Eq. (9), considering only the instantaneous ground states of the piecewise constant time-independent Hamiltonian, which corresponds to the adiabatic evolution of the system for the studied case. The results are summarized in Fig. 5. In all cases we recover our results corresponding to the slow limit, showing that our results persist in the adiabatic limit.

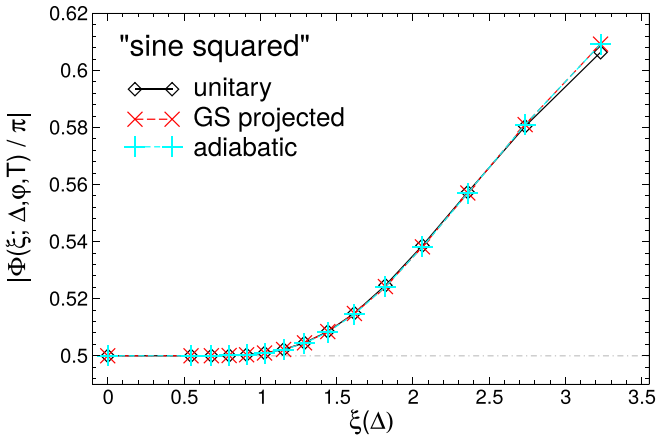

FIG. 5. Exchange phase $\Phi(\xi;\Delta,\varphi,T)$ vs MBS localization length $\xi(\Delta)$, for unitary (black diamonds), ground-state projected (cyan crosses), and adiabatic braiding process (blue pluses). As in Fig. 4, the braiding protocol is applied to a symmetric Y junction ($\varphi=\pi/3$) with equal-size legs $\ell=5$, using the sine-squared ramp with time period $T=750$ and $\alpha=0.025$. Data points (left to right) for each plot correspond to pairing amplitudes $\Delta=1.0,\ldots,0.3$ in steps of 0.05, which translates to increasing MBS localization length $\xi(\Delta)$ from left to right. Lines are guides to the eye.

IX. INTERACTIONS

Finally, we investigate the influence of a nearest-neighbor interaction $V\neq 0$ [see Eqs. (1) and (2)] on the braiding operation. In general, interactions in Majorana systems modify the localization length and change the bulk energy gap [41–43,45]. Large values of interaction strength V of either sign eliminate the topological phase. Here, we only consider values V for which the topological phase is not destroyed at $\mu=0$, and where $\mu=4$ is still large enough to drive the corresponding junction leg into the trivial phase. In Fig. 6, we plot the braiding phase $\Phi(V;\Delta,\varphi,T)$ and loss of fidelity $w^{e/o}_{\rm loss}(V;\Delta,\varphi,T)$ as a function of V. We consider a symmetric Y junction with equal-size legs $\ell=5$, now with pairing strengths $\Delta=1.0$, 0.8, and 1.1. We only show results for the sine-squared ramp function with $T=750$, which in the noninteracting case was found to be sufficient to ensure close-to-adiabatic conditions (cf. Fig. 4). The Majorana localization length $\xi(V;\Delta,L)$ is depicted for Kitaev chains of up to $L=22$ sites, and obtained by fitting the weights of the free fermionic representation of the MBS [42]. For the ideal parameter set $\Delta=J=1$, the Majorana localization length increases with either increasing repulsive or attractive interaction V. This effect turns out to be larger for an attractive potential, where $\xi>1$ for $|V|>0.35$, and the braiding phase starts to deviate significantly from $\pi/2$. For $\Delta=0.8$, the minimum of $\xi(V;\Delta=0.8,L)$ is shifted to $V\approx-0.35$, where for the given T one also observes a stabilization of the correct braiding phase. For large $\Delta=1.1$, the situation is reversed since then repulsive interactions lead to a reduction of the effective superconducting gap, pushing the system closer to the ideal point $\Delta_{\rm eff}=J$. The fidelity losses mainly depend on the braiding velocity $\sim\ell/T$, and hence remain of a similar magnitude for moderate V. As a weak trend, we find that small attractive or repulsive interactions play a stabilizing role for the braiding operation, depending on the relative size of the bare couplings J and Δ. Again, these effects appear not

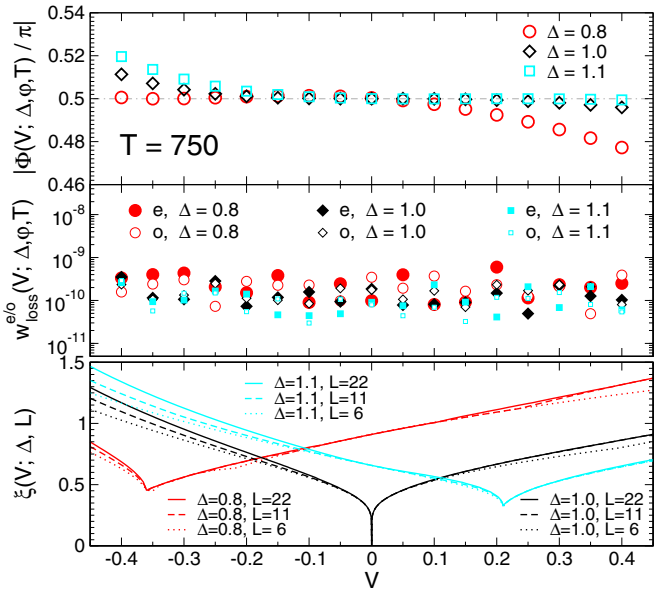

FIG. 6. Exchange phase $\Phi(V;\Delta,\varphi,T)$ (upper plot) and loss of fidelity $w_{\rm loss}^{e/o}(V;\Delta,\varphi,T)$ (middle plot) vs interaction strength V for pairing amplitudes $\Delta = 1.0$ (black diamonds), $\Delta = 0.8$ (red circles), and $\Delta = 1.1$ (cyan squares). As in Fig. 4, the braiding protocol is applied to a symmetric Y junction ($\varphi = \pi/3$) with equal-size legs $\ell = 5$, using the sine-squared ramp with time period $T = 750$ and $\alpha = 0.025$. The bottom plot shows the MBS localization length $\xi(V;\Delta,L)$ vs interaction strength V for a Kitaev chain with $L = 22$, 11, and 6 sites (solid, dashed, and dotted lines). Again, we consider pairing amplitudes $\Delta = 1.0$ (black), $\Delta = 0.8$ (red), and $\Delta = 1.1$ (cyan).

to be systematically encoded in spectral losses alone, which one can investigate by tracking the Majorana wave-function weights [54], but rather follow directly the behavior of the MBS localization length ξ (cf. both Figs. 4 and 6).

X. DISCUSSION AND CONCLUSIONS

Previous studies of Majorana braiding have predominantly focused on effective models of the low-energy (Majorana) sector [26,48], introducing nonadiabatic effects and other sources of errors on an effective but not microscopic level [47,50,51,67]. Alternatively, the fidelity of the dynamically evolved state was considered with respect to some ideal, adiabatic reference state [52–54]. Resulting estimates for the minimal protocol time for near-adiabatic time evolution in Majorana systems were obtained by many groups [50–54]. As an overarching implication, until recently, it was assumed that by just executing the braiding manipulations sufficiently slowly (but fast compared to the Majorana hybridization energy), one could recover the ideal operation completely. Those studies, however, explicitly disregard the generation and propagation of nonadiabatic excitations, which may occur not only due to an overall nonadiabacity of the braiding but also due to the lack of smoothness of the ramp function [56]. In turn, the propagation of (quasiparticle) excitations can directly affect the geometric braiding phase [55].

In our work, instead of further extending previous studies to more complex setups and protocols [29,52,53], we have revisited the most elementary case of a single MBS braiding operation in a Y junction of three Kitaev chains [26]. We considered the full Hilbert space, including the quasiparticle background beyond the low-energy Majorana sector, and investigated several error sources that destroy the perfect braiding phase during the nonadiabatic, unitary time evolution of the system. By adopting the Bargmann vertex formula for the geometric phase, customarily used in the characterization of geometric quantum gate operations [61], we identified explicitly the MBS braiding phase, and analyzed its behavior during the braid. We then accounted for both spectral losses (through the fidelity) and direct braiding phase errors (by calculating the geometric phase evolution explicitly) in a numerically exact framework, in order to understand in detail how nonadiabacity, the Majorana mode localization, and interactions affect the braiding operation.

We find that due to the induced nonadiabatic leakage of wave-function weight out of the ground state into excited states of the final Hamiltonian, the acquired braiding phase does not remain constant and evolves linearly in time even after the braiding process is finished (cf. Fig. 2). Consequently, the final (qubit) state will "dephase" with time, even in the zero-temperature case considered here. While spectral losses can be reduced by orders of magnitude through increasing the ramping time period T or considering smoother ramp functions (cf. Fig. 4), it is clear that in extended protocols necessary for serious quantum computations, nonadiabatic errors will accumulate. Our results, based on a numerically exact treatment of the full Hilbert space, thus support and extend the findings of Pedrocchi and DiVincenzo [55] and Knapp *et al.* [56] that employed an effective description of the low-energy Majorana sector (including the quasiparticle background via baths/dissipation).

By varying the superconducting wire bulk gap, we additionally resolved how the localization length of individual Majorana zero modes affects the braiding operation, beyond simple dynamical errors induced through a finite MBS hybridization [47,54]. For the studied Y-junction configuration in Fig. 1, a MBS localization length $\xi > 1$ already causes significant deviations from the perfect braiding phase $\pi/2$, since the independent-particle picture of Majorana braiding [7,8,26] breaks down. We emphasize that this finite-size breakdown occurs independent of adiabacity (cf. Fig. 4). It implies that measures of adiabacity—such as the fidelity or Majorana wave-function weights alone—may suggest overoptimistic efficiencies of the braiding operation. At the same time, the behavior in Fig. 4 shows how an extraction of the geometric phase Eq. (9) can yield valuable information about the anyonic statistics encoded in the many-body states of a complex system. Finally, the nearest-neighbor interaction in the wires is found to predominantly affect the braiding operation through its impact on the wire bulk gap. Depending on the noninteracting gap versus hopping strength, for weak attractive (repulsive) interactions, the braiding operation is more stable due to a change of the effective superconducting gap and the reduction of the MBS localization length (cf. Refs. [41–43]).

In summary, finite operation times and nonideal parameter settings in (simple) Majorana braiding schemes pose serious

constraints on the accuracy of braiding operations. We found that even for the ideal case of a closed, zero-temperature Kitaev chain system, nonadiabatic errors and finite Majorana hybridization can become bottlenecks for the fidelity and feasibility of (extended) Majorana braiding routines towards quantum computation. An accumulation of nonadiabatic errors has to be avoided, likely leading to unfavorable finite-time scaling if no explicit quasiparticle relaxation mechanism is included. The optimal engineering of dissipation out of the excited-state sector, such as the trapping of quasiparticles, as well as measurement-based (dissipative) topological quantum computation schemes [33–35] may thus behave favorably in comparison to conventional adiabatic-manipulation schemes [26,29,30] (cf. Ref. [56]). Similarly, finite Majorana overlaps have to be avoided to high accuracy, since these directly affect the braiding statistics encoded in the low-energy sector of the system—in fact, the braiding statistics become "non-Majorana" (cf. Fig. 4 and the discussion). As an order of magnitude comparison, we note that current-date nanowire and iron-chain architectures [21–25] find localization versus device lengths of $\xi/L \simeq 0.2 \ldots 1$, where our numerics indicate that assuming individual Majoranas (in terms of their braiding statistics) might be too optimistic. Advancing towards longer nanowire devices or a reduction of the MBS localization length, also for the sake of measurement-based qubit experiments [33–35], is thus clearly desirable.

In the end, our results nevertheless show that for long enough wires (or short enough MBS localization lengths), and for reasonably smooth and adiabatic protocols, ideal Majorana braiding might be observed. An analysis of braiding and computation protocols in extended Majorana wire networks [31–35] will be subject to future work, using more sophisticated techniques applicable to larger system sizes. Clearly, these measurement-based schemes for topological quantum computation should face the same detailed numerical investigation and scrutiny as the direct braiding and adiabatic-manipulation schemes.

ACKNOWLEDGMENTS

We thank A. Akhmerov, M. Burrello, R. Egger, S. Frolov, T. Karzig, and R. Lutchyn for fruitful discussions. This work was supported by DFG-SFB 1170 and ERC-StG-Thomale-TOPOLECTRICS-336012. M.S. acknowledges support by the Rustaveli National Science Foundation through Grant No. FR/265/6-100/14.

[1] J. Alicea, Rep. Prog. Phys. **75**, 076501 (2012).
[2] M. Leijnse and K. Flensberg, Semicond. Sci. Technol. **27**, 124003 (2012).
[3] C. W. J. Beenakker, Annu. Rev. Condens. Matter Phys. **4**, 113 (2013).
[4] S. D. Sarma, M. Freedman, and C. Nayak, npj Quantum Inf. **1**, 15001 (2015).
[5] G. Moore and N. Read, Nucl. Phys. B **360**, 362 (1991).
[6] N. Read and D. Green, Phys. Rev. B **61**, 10267 (2000).
[7] A. Y. Kitaev, Phys. Usp. **44**, 131 (2001).
[8] D. A. Ivanov, Phys. Rev. Lett. **86**, 268 (2001).
[9] A. Kitaev, Ann. Phys. **321**, 2 (2006).
[10] M. Greiter and R. Thomale, Phys. Rev. Lett. **102**, 207203 (2009).
[11] L. Fu and C. L. Kane, Phys. Rev. Lett. **100**, 096407 (2008).
[12] R. M. Lutchyn, J. D. Sau, and S. Das Sarma, Phys. Rev. Lett. **105**, 077001 (2010).
[13] Y. Oreg, G. Refael, and F. von Oppen, Phys. Rev. Lett. **105**, 177002 (2010).
[14] S. Nadj-Perge, I. K. Drozdov, B. A. Bernevig, and A. Yazdani, Phys. Rev. B **88**, 020407(R) (2013).
[15] V. Mourik, K. Zuo, S. M. Frolov, S. R. Plissard, E. P. A. M. Bakkers, and L. P. Kouwenhoven, Science **336**, 1003 (2012).
[16] L. P. Rokhinson, X. Liu, and J. K. Furdyna, Nat. Phys. **8**, 795 (2012).
[17] A. Das, Y. Ronen, Y. Most, Y. Oreg, M. Heiblum, and H. Shtrikman, Nat. Phys. **8**, 887 (2012).
[18] M. T. Deng, C. L. Yu, G. Y. Huang, M. Larsson, P. Caroff, and H. Q. Xu, Nano Lett. **12**, 6414 (2012).
[19] H. O. H. Churchill, V. Fatemi, K. Grove-Rasmussen, M. T. Deng, P. Caroff, H. Q. Xu, and C. M. Marcus, Phys. Rev. B **87**, 241401(R) (2013).
[20] S. Nadj-Perge, I. K. Drozdov, J. Li, H. Chen, S. Jeon, J. Seo, A. H. MacDonald, B. A. Bernevig, and A. Yazdani, Science **346**, 602 (2014).
[21] S. M. Albrecht, A. P. Higginbotham, M. Madsen, F. Kuemmeth, T. S. Jespersen, J. Nygård, P. Krogstrup, and C. M. Marcus, Nature (London) **531**, 206 (2016).
[22] M. T. Deng, S. Vaitiekenas, E. B. Hansen, J. Danon, M. Leijnse, K. Flensberg, J. Nygård, P. Krogstrup, and C. M. Marcus, Science **354**, 1557 (2016).
[23] R. Pawlak, M. Kisiel, J. Klinovaja, T. Meier, S. Kawai, T. Glatzel, D. Loss, and E. Meyer, npj Quantum Inf. **2**, 16035 (2016).
[24] B. E. Feldman, M. T. Randeria, J. Li, S. Jeon, Y. Xie, Z. Wang, I. K. Drozdov, B. A. Bernevig, and A. Yazdani, Nat. Phys. **13**, 286 (2017).
[25] H. Zhang *et al.*, Nat. Commun. **8**, 16025 (2017).
[26] J. Alicea, Y. Oreg, G. Refael, F. von Oppen, and M. P. A. Fisher, Nat. Phys. **7**, 412 (2011).
[27] B. van Heck, A. R. Akhmerov, F. Hassler, M. Burrello, and C. W. J. Beenakker, New J. Phys. **14**, 035019 (2012).
[28] J. Li, T. Neupert, B. A. Bernevig, and A. Yazdani, Nat. Commun. **7**, 10395 (2016).
[29] D. Aasen, M. Hell, R. V. Mishmash, A. Higginbotham, J. Danon, M. Leijnse, T. S. Jespersen, J. A. Folk, C. M. Marcus, K. Flensberg, and J. Alicea, Phys. Rev. X **6**, 031016 (2016).
[30] T. Hyart, B. van Heck, I. C. Fulga, M. Burrello, A. R. Akhmerov, and C. W. J. Beenakker, Phys. Rev. B **88**, 035121 (2013).
[31] L. A. Landau, S. Plugge, E. Sela, A. Altland, S. M. Albrecht, and R. Egger, Phys. Rev. Lett. **116**, 050501 (2016).
[32] S. Plugge, L. A. Landau, E. Sela, A. Altland, K. Flensberg, and R. Egger, Phys. Rev. B **94**, 174514 (2016).

[33] S. Plugge, A. Rasmussen, R. Egger, and K. Flensberg, New J. Phys. **19**, 012001 (2017).
[34] S. Vijay and L. Fu, Phys. Rev. B **94**, 235446 (2016).
[35] T. Karzig, C. Knapp, R. M. Lutchyn, P. Bonderson, M. B. Hastings, C. Nayak, J. Alicea, K. Flensberg, S. Plugge, Y. Oreg, C. M. Marcus, and M. H. Freedman, Phys. Rev. B **95**, 235305 (2017).
[36] S. Hoffman, C. Schrade, J. Klinovaja, and D. Loss, Phys. Rev. B **94**, 045316 (2016).
[37] S. Vijay, T. H. Hsieh, and L. Fu, Phys. Rev. X **5**, 041038 (2015).
[38] S. Vijay and L. Fu, Phys. Scr. **T168**, 014002 (2016).
[39] C. V. Kraus, P. Zoller, and M. A. Baranov, Phys. Rev. Lett. **111**, 203001 (2013).
[40] C. Laflamme, M. A. Baranov, P. Zoller, and C. V. Kraus, Phys. Rev. A **89**, 022319 (2014).
[41] S. Gangadharaiah, B. Braunecker, P. Simon, and D. Loss, Phys. Rev. Lett. **107**, 036801 (2011).
[42] E. M. Stoudenmire, J. Alicea, O. A. Starykh, and M. P. A. Fisher, Phys. Rev. B **84**, 014503 (2011).
[43] E. Sela, A. Altland, and A. Rosch, Phys. Rev. B **84**, 085114 (2011).
[44] F. Hassler and D. Schuricht, New J. Phys. **14**, 125018 (2012).
[45] R. Thomale, S. Rachel, and P. Schmitteckert, Phys. Rev. B **88**, 161103(R) (2013).
[46] M. Greiter, V. Schnells, and R. Thomale, Ann. Phys. **351**, 1026 (2014).
[47] M. Cheng, V. Galitski, and S. Das Sarma, Phys. Rev. B **84**, 104529 (2011).
[48] D. J. Clarke, J. D. Sau, and S. Tewari, Phys. Rev. B **84**, 035120 (2011).
[49] B. I. Halperin, Y. Oreg, A. Stern, G. Refael, J. Alicea, and F. von Oppen, Phys. Rev. B **85**, 144501 (2012).
[50] T. Karzig, G. Refael, and F. von Oppen, Phys. Rev. X **3**, 041017 (2013).
[51] M. S. Scheurer and A. Shnirman, Phys. Rev. B **88**, 064515 (2013).
[52] T. Karzig, A. Rahmani, F. von Oppen, and G. Refael, Phys. Rev. B **91**, 201404 (2015).
[53] T. Karzig, F. Pientka, G. Refael, and F. von Oppen, Phys. Rev. B **91**, 201102(R) (2015).
[54] C. S. Amorim, K. Ebihara, A. Yamakage, Y. Tanaka, and M. Sato, Phys. Rev. B **91**, 174305 (2015).
[55] F. L. Pedrocchi and D. P. DiVincenzo, Phys. Rev. Lett. **115**, 120402 (2015).
[56] C. Knapp, M. Zaletel, D. E. Liu, M. Cheng, P. Bonderson, and C. Nayak, Phys. Rev. X **6**, 041003 (2016).
[57] V. Khemani, R. Nandkishore, and S. L. Sondhi, Nat. Phys. **11**, 560 (2015).
[58] M. A. Nielsen and I. L. Chuang, *Quantum Computation and Quantum Information* (Cambridge University Press, Cambridge, UK, 2000).
[59] M. V. Berry, Proc. R. Soc. London, Ser. A **392**, 45 (1984).
[60] J. Samuel and R. Bhandari, Phys. Rev. Lett. **60**, 2339 (1988).
[61] N. Mukunda and R. Simon, Ann. Phys. **228**, 205 (1993).
[62] An equivalence class of states in ray space is a projection operator $|\psi\rangle\langle\psi|$ to the equivalence class represented by $|\psi\rangle$. This is a natural projection that maps each vector to the ray on which it lies.
[63] Y. Aharonov and J. Anandan, Phys. Rev. Lett. **58**, 1593 (1987).
[64] M. Sadkane and R. B. Sidje, Numer. Algorithms **20**, 217 (1999).
[65] C. Moler and C. V. Loan, SIAM Rev. **45**, 3 (2003).
[66] M. Moliner and P. Schmitteckert, Phys. Rev. Lett. **111**, 120602 (2013).
[67] I. C. Fulga, B. van Heck, M. Burrello, and T. Hyart, Phys. Rev. B **88**, 155435 (2013).